

A Very Slow Creep Test on an Avery Island Salt Sample

P. Bérest¹ · J. F. Béraud¹ · H. Gharbi¹ · B. Brouard² · K. DeVries³

Received: 8 September 2015 / Accepted: 9 September 2015 / Published online: 21 September 2015
© Springer-Verlag Wien 2015

Abstract The applied deviatoric stress during most creep tests performed on salt samples is in the 3.5–20 MPa range. However, the stresses actually experienced in the vicinity of a salt cavern are much smaller. Any extrapolation is difficult to vindicate, as the dominant micro-mechanisms are strongly suspected to be very different in the low-stress and medium-stress domains. To answer this concern, a very slow creep test was performed on an Avery Island salt sample. To minimize the influence of even the smallest of temperature deviations during the test, the testing apparatus was placed in a remote gallery of the Varangéville salt mine, taking advantage of the very stable temperature conditions offered in an underground environment. The test was performed in multiple stages and lasted 42 months. The successive loads of 0.1, 0.2, 0.3, and 0.5 MPa were applied. Measured steady-state strain rates were of the order of 10^{-12} s^{-1} , which are significantly faster than that extrapolated from creep tests performed at loads ranging between 3.5 and 20 MPa.

Keywords Salt creep · Creep test · Slow strain rate

Latin Symbols

a	Cavern radius (m)
A	Parameter of the steady-state creep law (Pa^{-n}/s)
c	Parameter of the transient constitutive law (K^{-1})
D	Diameter of a cylindrical sample (m)
E	Young's modulus (Pa)
J_2	Second invariant of the deviatoric stress tensor (Pa)
k_{salt}	Thermal diffusivity of salt (m^2/s)
K_0	Parameter of the transient constitutive law (Pa^{-m})
m	Exponent of stress in the transient constitutive law (–)
n	Exponent of stress in the steady-state creep law (Pa)
p	Parameter of the transient constitutive law (–)
P	Cavern internal pressure (Pa)
P_{atm}	Atmospheric pressure (Pa)
P_h	Halmostatic pressure (Pa)
P_∞	Geostatic pressure (Pa)
q	Parameter of the constitutive law (–)
Q/R	Parameter of the steady-state creep law (K^{-1})
r	Distance to the axis of symmetry (m)
s_{ij}	Components of the deviatoric stress tensor (Pa)
t	Time (s)
t_c	Characteristic time for heat conduction (s)
T	Absolute temperature (K)
u	Vertical displacement (m)
w	Parameter of the constitutive law (–)

Greek Symbols

α	Thermal expansion coefficient (K^{-1})
γ	Ratio of the heat capacities of a perfect gas (–)
δ_{ij}	Kronecker tensor
Δ	Parameter of the transient constitutive law (–)
$\Delta\sigma$	Deviatoric stress change (Pa)
ΔT	Temperature change (K)
ε	Strain (–)

✉ P. Bérest
berest@lms.polytechnique.fr

¹ LMS, Ecole Polytechnique, Palaiseau, France

² Brouard Consulting, Paris, France

³ RESPEC, Rapid City, SD, USA

ε_t^*	Asymptotic value of the transient strain (—)
$\dot{\varepsilon}$	Strain rate (s^{-1})
$\dot{\varepsilon}_s$	Steady-state strain rate (s^{-1})
$\dot{\varepsilon}_t$	Transient strain rate (s^{-1})
$\dot{\varepsilon}_{vp}$	Viscoplastic strain rate (s^{-1})
ζ	Internal parameter of the constitutive law (—)
θ	Characteristic time of the constitutive law (s)
σ	Deviatoric stress (Pa)
σ_1	Deviatoric stress first step (Pa)
σ_2	Deviatoric stress second step (Pa)
σ_{ij}	Components of the stress tensor (Pa)
σ_{zz}	Axial stress (Pa)
Φ	Relative humidity (%)

1 Introduction

A rock mechanics study is typically required before commissioning caverns for salt production or hydrocarbon storage. Constitutive laws for rock salt are used; they are based on empirical data provided by creep tests performed in the laboratory. Abundant literature has been dedicated to the various aspects of the creep behavior of salt, see for instance the proceedings of the eight conferences on the Mechanical Behavior of Salt.

During most laboratory tests, the applied deviatoric stress is in the 5–20 MPa range. However, computations prove, in many cases, that the deviatoric stresses actually experienced in the vicinity of caverns are smaller than 5 MPa. In other words, computations are based on extrapolation of laboratory tests performed in a stress range which is not the stress range of direct interest. Several field and laboratory tests indicate that such an extrapolation drastically underestimates the actual creep rate of rock salt. As a consequence, numerical computations based on creep tests performed in the laboratory can significantly underestimate cavern closure rate, especially in shallow (less than 1000 m deep) caverns.

Tests performed in the range of deviatoric stresses that match field conditions are scarce because strain rates during these tests are exceedingly slow ($10^{-12}/s$, i.e., $3.10^{-5}/$ year): daily room temperature fluctuations generate thermoelastic strains which are much larger than the strains to be measured. This problem can be solved two ways. The first consists of designing a special testing device in which temperature fluctuations are made quite small. Such a device was built and operated by Hunsche (1988). The second resolution consists of setting the testing device in an environment with exceedingly small temperature fluctuations, for instance, a dead-end mine drift, Bérest et al. (2005). This paper is dedicated to a multi-step creep test performed in a drift on a salt sample cored from the Avery Island Mine in Louisiana.

2 Extrapolation of Creep-Test Results to Small Stresses

2.1 Laboratory Creep Tests

This paper focuses on the remarkably slow strain rates determined from a creep test performed on a rock salt sample subject to relatively small deviatoric stresses. It generally is accepted (e.g., Bérest 2013) that the axial strain (ε) observed during a creep test performed on a cylindrical-shaped salt specimen in the laboratory, is the sum of three components: the thermoelastic strain, the transient viscoplastic strain (ε_t), and the steady-state viscoplastic strain (ε_s), as shown in Fig. 1 and mathematically expressed in one-dimensional rate form as

$$\dot{\varepsilon} - \frac{\dot{\sigma}_{zz}}{E} + \alpha \dot{T} = \dot{\varepsilon}_{vp} = \dot{\varepsilon}_s + \dot{\varepsilon}_t, \quad (1)$$

where contractive strains and compressive stresses are positive, σ_{zz} is the applied stress during a uniaxial test, E is Young's modulus, and α is the thermal expansion coefficient. Eq. 1 does not include the possible influence of hygrometry changes which is discussed in Sect. 2.2.

Total viscoplastic strain (ε_{vp}) is the sum of transient and steady-state components.

The steady-state viscoplastic component contribution to the total deformation is typically defined as a constant strain rate, $\dot{\varepsilon}_s$, reached after several weeks or months when the temperature and the deviatoric stress are kept constant. For rock salt, steady-state strain rates are a function of shear stress and temperature. A simple formulation for a steady-state creep law is given by

$$\dot{\varepsilon}_s = A \exp(-Q/RT) \sigma^n \text{ (Norton - Hoff)} \quad (2)$$

where σ^n is the applied stress during a uniaxial test (or, more generally, $\sigma = \sqrt{3J_2}$ where $J_2 = s_{ij}s_{ji}/2$ is the second

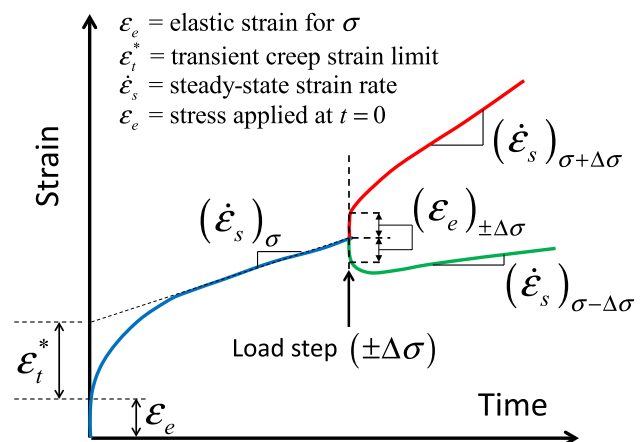


Fig. 1 Strain as a function of time during a creep test. (Van Sambeek et al. 1993)

invariant of the deviatoric stress tensor, $s_{ij} = \sigma_{ij} - \sigma_{kk}\delta_{ij}/3$, T is absolute temperature, and A , Q , and n are three constants, with n in the 3–6 range and the thermal constant, Q/R , in the 3000–10,000 K domain.

At ambient temperature and at a deviatoric stress of $\sigma = 10$ MPa, the steady-state strain rate for salt is typically about $\dot{\epsilon}_s = 10^{-10}\text{s}^{-1}$. For instance, Avery Island salt has been studied extensively by RESPEC, and the results of approximately 55 RESPEC creep tests are represented in a $\log|\sigma|$ versus $\log|\dot{\epsilon}_s|$ plot in Fig. 2. In principle, the mean stress has no influence on steady-state strain rate, and no volumetric change is observed for typical confining pressures used for most triaxial creep tests. However, dilation is often exhibited under low or moderate confining pressures and high shear stresses with the propensity for dilation increasing for progressively lower confining pressures and greater shear stresses.

The transient component describes the rock viscoplastic behavior before steady state is reached. Any change in applied loading ($\Delta\sigma$) or temperature (ΔT) triggers a transient creep response. Following a load increase (“direct creep”), transient creep is characterized by relatively faster initial strain rates compared to the steady-state strain rates. Similarly, slower initial rates—or even “reverse” initial strain rates follow a load decrease; i.e., the specimen strains in the opposite direction of the applied load—are exhibited following a “stress drop” (Fig. 1). If the applied stress is kept constant after the stress change, the transient rate slowly decreases (or increases) until the transient strain exhausts itself; i.e., the total strain rate becomes equal to the steady-state rate. In theory, the transient strain reaches

an asymptotic value defined as the transient strain limit $\epsilon_t^* = \epsilon_t^*(\sigma, T)$ that is a function of deviatoric stress and temperature. Munson et al. (1996) suggest the transient strain limit is an exponential function of temperature and a power function of shear stress and three material constants, K_0 , c , and m :

$$\epsilon_t^* = K_0 e^{cT} \sigma^m \tag{3}$$

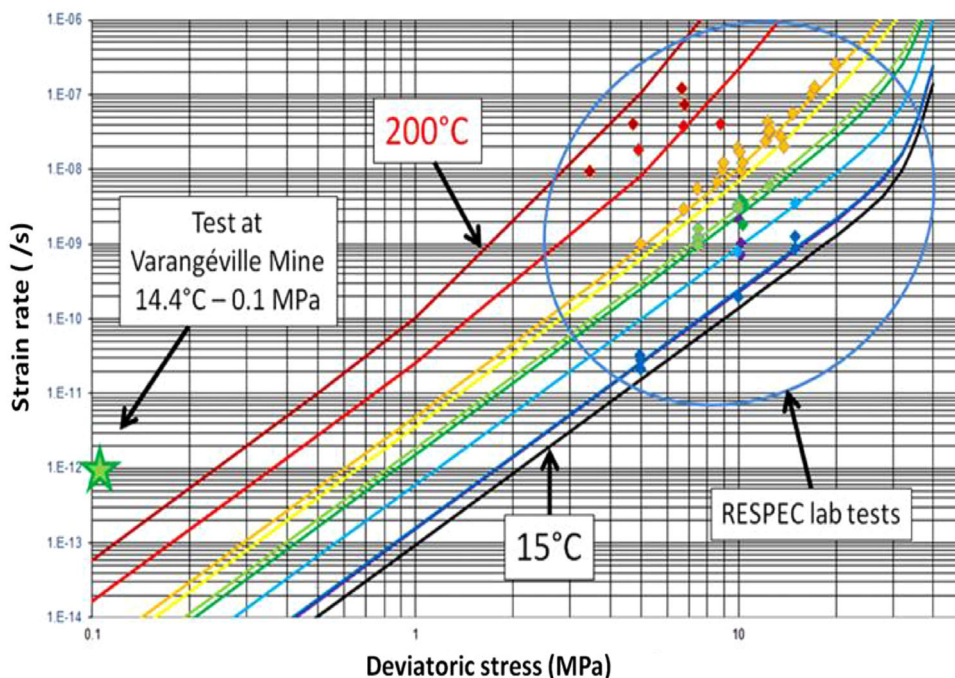
A characteristic time, θ , can be defined as the time after which, for given σ and T , the accumulated steady-state strain, $\dot{\epsilon}_s \theta$, is larger than the asymptotic transient strain, ϵ_t^* :

$$\theta(\sigma, T) = \epsilon_t^* / \dot{\epsilon}_s = K_0 e^{cT+Q/RT} \sigma^{n-m} / A \tag{4}$$

Djizanne-Djakeun (2014) estimated values of θ from a dozen different salt formations at $\sigma = 10$ MPa and $T = 310$ K. The values for θ typically range between 0.5 and 5 years. Munson et al. (1996) proposed an internal variable, ζ , to describe the transient strain, which slowly increases (or decreases) to reach the transient strain limit $\epsilon_t^* = \epsilon_t^*(\sigma, T)$ when σ and T are kept constant. For instance, during a uniaxial creep test, Munson et al. (1996) proposed $\dot{\epsilon}_{vp} = \dot{\epsilon}_s + \dot{\zeta}$; when $\zeta/\epsilon_t^* < 1$, $\dot{\zeta}/\dot{\epsilon}_s = \exp[\Delta(1 - \zeta/\epsilon_t^*)^2] - 1$, where Δ is a function of σ . Similarly, Bérest et al. (2007) proposed $\dot{\zeta}/\dot{\epsilon}_s = -(\zeta/\epsilon_t^* - 1)^p / (k - 1)^p$ when $\zeta/\epsilon_t^* > 1$. Reverse creep appears, $\dot{\epsilon}_s + \dot{\zeta} < 0$, when $\zeta/\epsilon_t^* > k > 1$.

Although other formulations can be selected, Munson’s constitutive law captures the main features of both transient and steady-state creep behavior, and it will be used for interpretation, at least in a qualitative way, of the main results of the creep test reported herein.

Fig. 2 Steady-state strain rate as a function of deviatoric stress and temperature for Avery Island salt



2.2 Deviatoric Stresses at a Cavern Wall

As previously stated, when $\sigma = 10\text{MPa}$ and $T = 310\text{K}$, the steady-state strain rate is approximately 10^{-10}s^{-1} . Assuming a typical value of 4 for the exponent of the Norton-Hoff law, n , this law predicts that the steady-state strain rate should be approximately 10^{-14}s^{-1} (3×10^{-7} /year) when $\sigma = 1\text{MPa}$. As discussed later, this rate is too slow to be measured in rock mechanics laboratories. For this reason, most creep tests are performed in the $\sigma = 5\text{--}20\text{MPa}$ range (Fig. 2), at least when the temperature is lower than $50\text{ }^\circ\text{C}$. However, this stress range does not capture the expected state of stress surrounding a salt cavern.

When the Norton-Hoff law is used to compute the behavior of a relatively shallow salt cavern, it is observed that the deviatoric stresses in the vicinity of the cavern are smaller than 5MPa . Consider, for instance, the 750m deep cavern having the shape represented in Fig. 3. During the simulated leaching period, which lasts 600 days , cavern pressure is progressively lowered from geostatic pressure to halmostatic pressure (the cavern pressure when the access borehole is filled with saturated brine of density 1200 kg/m^3). Thereafter, the pressure is kept constant for 2400 days ; the stresses in the salt at 600 days , when the cavern is at halmostatic pressure, are slightly greater than 5MPa . After the cavern is held stagnant for an additional 2400 days , the deviatoric stresses are less than 5MPa in almost the entire rock mass, except in few overhanging parts at the cavern wall.

Consider also an idealized cylindrical cavern whose internal pressure abruptly decreases at time $t = 0$ from geostatic pressure, $P = P_\infty$, to halmostatic pressure, $P = P_h$. At $t = 0$ and $t = \infty$ (steady state), the deviatoric stress is

$$\begin{cases} \sqrt{3}J_2|^{t=0} = \sqrt{3}(P_\infty - P_h)(a/r)^2/2 \\ \sqrt{3}J_2|^{t=\infty} = \sqrt{3}(P_\infty - P_h)(a/r)^{2/n}/2n \end{cases} \quad (5)$$

where r is the distance to the axis of symmetry, and a is the cavern radius. The maximum deviatoric stress at time zero and at steady state occurs at the cavern wall. The steady-state deviatoric stress is smaller than the initial deviatoric stress by a factor of n . Hence, for increasingly greater values for the exponent of the Norton-Hoff law, the steady-state deviatoric stresses are progressively smaller. In a 750-m -deep cavern, the deviatoric stress at the cavern wall is 6.5MPa at $t = 0$; when steady state is reached, it is 1.6MPa , assuming the exponent of the power law is $n = 4$. In other words, standard laboratory tests are not performed in the range of deviatoric stress that is relevant when computing the behavior of a brine-filled salt cavern. The question becomes: Is extrapolation acceptable?

2.3 Deformation Mechanism

Langer (1984) stated that reliable extrapolation of the creep equations at low deformation rates can be carried out only on the basis of deformation mechanisms. The micro-mechanisms that govern salt creep have been discussed by Langer (1984), Munson and Dawson (1984), and Blum and Fleischman (1988). A deformation-mechanism map (adapted from Munson and Dawson 1984) is presented in Fig. 4. The temperature and stress ranges ($0\text{--}120\text{ }^\circ\text{C}$ by $5\text{--}20\text{MPa}$) in which most laboratory tests are performed are identified in Fig. 4. The micro-mechanisms that govern creep in the domain $\sigma = 0\text{--}5\text{MPa}$, which is of primary interest, are unknown. Therefore, prediction of the

Fig. 3 Deviatoric-stress contours after 600 days (left) and 3000 days (right)

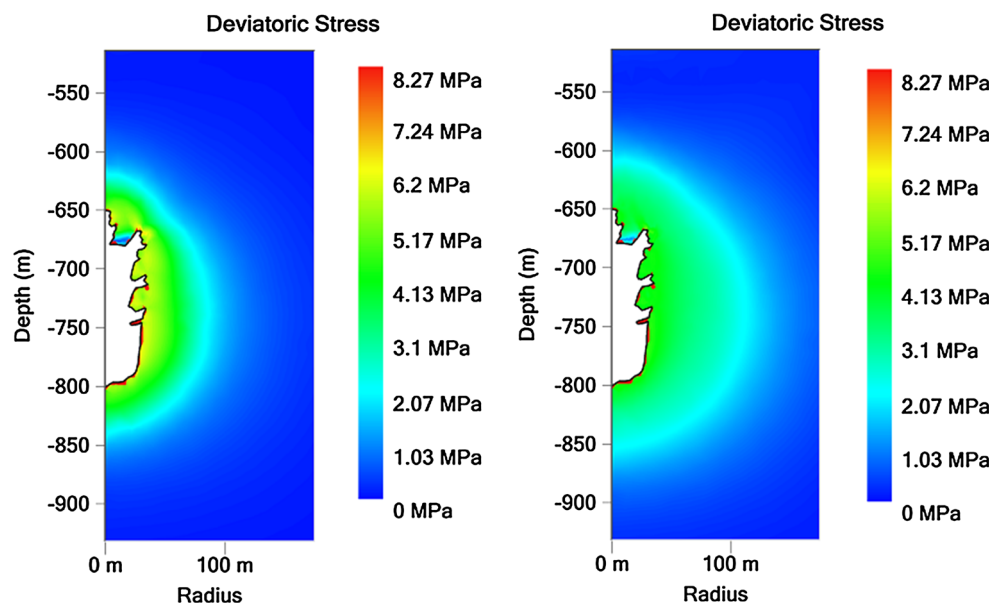
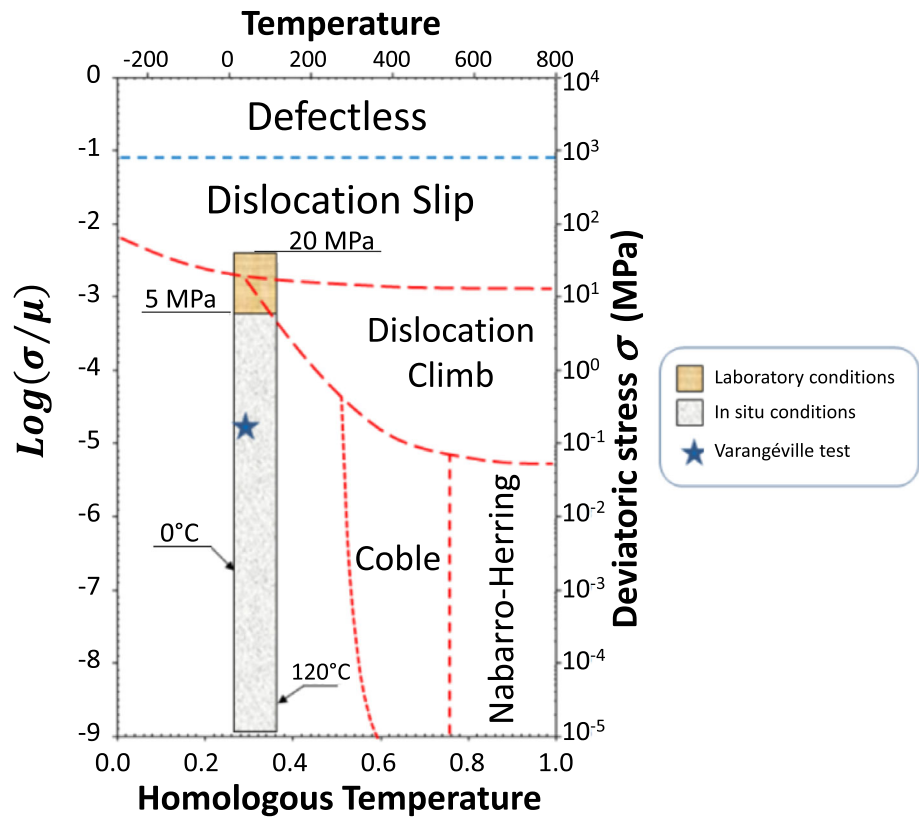


Fig. 4 Micro-mechanism map (after Munson and Dawson 1984)



mechanical behavior of salt in this domain is based on extrapolation of purely empirical data and cannot be supported by theoretical consideration.

However, Spiers et al. (1990) and Uraï and Spiers (2007) observed that in the low-stress domain, pressure-resolution creep, which is an important deformation mechanism of most rocks in the earth’s crust, is especially rapid in the case of rock salt. Theoretical findings strongly suggest that, for this mechanism, the relation between deviatoric stress and strain rate is linear, with important consequences for computing both geological processes and the operation of underground workings.

3 Problems Raised by Slow-Rate Creep Tests

Slow strain rates ($\dot{\epsilon} \approx 10^{-14} - 10^{-11} \text{ s}^{-1}$) have not been investigated widely in the laboratory. The limited available literature is inherent to the particular problems raised by long-term, slow-rate creep tests as noted below.

3.1 Temperature

When performing accurate creep tests, temperature fluctuations are by far the main concern. Consider a test such that the applied stress is controlled perfectly. When steady state is reached, Eq. (1) is rewritten as

$$\dot{\epsilon} + \alpha \dot{T} = \dot{\epsilon}_s. \tag{6}$$

If the creep rate is approximately 10^{-12} s^{-1} , a test lasting 36 days ($3 \times 10^6 \text{ s}$) results in an accumulated viscoplastic strain of approximately 3×10^{-6} . The thermal expansion coefficient, α , of salt is approximately $4 \times 10^{-5} / ^\circ\text{C}$. If room temperature at the end of the test is warmer than at the beginning of the test by $0.1 \text{ } ^\circ\text{C}$, then the thermal strain ($\alpha \Delta T = 4 \times 10^{-6}$) is larger than the accumulated viscoplastic strain. In a standard laboratory testing room, avoiding temperature fluctuations as small as $0.1 \text{ } ^\circ\text{C}$ is practically impossible and wrong conclusions may be drawn from the test results.

This problem can be solved in two ways. The first consists of designing a special testing device in which temperature fluctuations are made quite small. Such a device was built and operated by Hunsche (1988). In a test using the specially designed device that lasted approximately 1 week, “the lowest reliably determined deformation rate” was $7 \times 10^{-12} \text{ s}^{-1}$. Temperature fluctuations were as low as $0.001 \text{ } ^\circ\text{C}$. The main drawback of this system is the cost to develop the environmental control chamber. The second resolution consists of setting the testing device in an environment with exceedingly small temperature fluctuations (e.g., a dead-end mine drift). Bérest et al. (2005) performed a series of uniaxial compression tests in a remote gallery of the Varangéville salt

mine. The applied stress was 0.1MPa, and the measured steady-state creep rate was found to be approximately 10^{-12} s^{-1} . The main drawback of this approach is that the testing temperature cannot be varied.

3.2 Hygrometry

Hygrometric variations can also be a concern (Horseman 1988; Hunsche and Schultze 1996, 2002; Van Sambeek 2012). Hunsche and Schultze (1996), for instance, suggested that when hygrometry is taken into account, the steady-state creep rate must be corrected as follows:

$$\dot{\varepsilon}_s = A[1 + w \sinh(q\Phi)] \exp(-Q/RT)\sigma^n, \quad (7)$$

where $0 < \Phi < 100$ is the relative hygrometry in the drift given as a percentage and the two constants (q and w) both have a value of 0.01. A change in room hygrometry from $\Phi = 55 \%$ RH to $\Phi = 75 \%$ RH leads to a factor of 7 increase in the steady-state rate.

3.3 Loading

Slow strain rates are typically obtained when small mechanical loadings are applied. Most creep-test devices for rock salt are designed to operate in the deviatoric stress range between 5 and 20 MPa. Stress control usually becomes poor when the applied stress is smaller than approximately 5 MPa. For example, Wawersik and Preece (1984) describe a creep test performed with an initial applied deviatoric stress of approximately 7 MPa that yielded an average strain rate of $2.5 \times 10^{-10} \text{ s}^{-1}$. Stress control was poor during this test and a 2.21 MPa spike in the applied stress was observed after 3550 h (Fig. 5); 56 h later, the stress was again equal to approximately 7 MPa, and over the next several weeks, the average strain rate was approximately $5.6 \times 10^{-11} \text{ s}^{-1}$ —four times slower than before the spike.

This effect is captured easily by the transient model described in Sect. 1.1. Before the stress spike, the deviatoric stress, denoted as σ_1 , was relatively constant, and an apparent steady state was reached; the internal variable, $\zeta(\sigma_1) = \zeta_1$, was equal to the transient strain limit, $\varepsilon_t^*(\sigma_1) = \varepsilon_{t1}^*$, for the constant test temperature. When the applied load abruptly increased from σ_1 to σ_2 at $t = t_1$, the rate of the internal variable experiences a drastic jump, $\dot{\zeta}/\dot{\varepsilon}_s^*(\sigma_2) = \exp[\Delta(\sigma_2) \times (1 - \zeta_1/\varepsilon_t^*(\sigma_2))^2] - 1$. When the sample is unloaded from σ_2 to σ_1 at $t = t_2$, the value of internal variable ζ_2 is significantly larger than the transient strain limit at the lower stress condition, $\varepsilon_t^*(\sigma_1) = \varepsilon_{t1}^*$, and the evolution of the internal parameter is governed by $\dot{\zeta}/\dot{\varepsilon}_s(\sigma_1) = -(\zeta/\varepsilon_{t1}^* - 1)^P/(k - 1)^P$. The creep rate

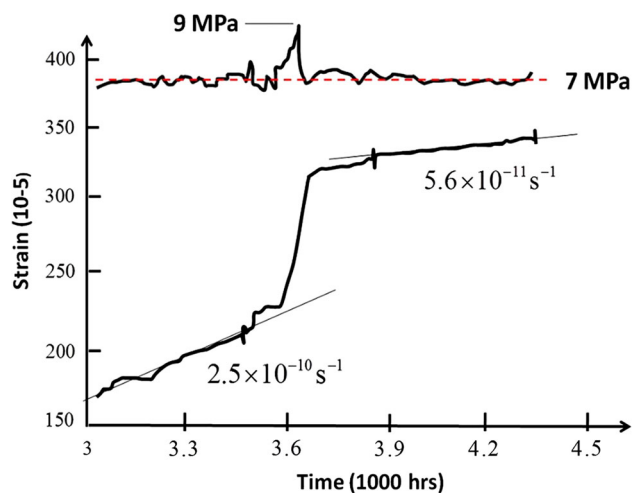


Fig. 5 Partial creep curves for poor stress control with superimposed stress-time records (after Wawersik and Preece 1984)

remains consistently slower than it was before the jump as shown in Fig. 5. This asymmetry in transient behaviors is responsible for the effect described by Wawersik and Preece (1984) and explains why stress control is of utmost importance.

3.4 Measurement of Axial Displacement

Creep rate is computed by comparing strains $\varepsilon_1 = \delta h_1/h$ and $\varepsilon_2 = \delta h_2/h$ measured at two different times, t_1 and t_2 , or $\dot{\varepsilon} = (\varepsilon_2 - \varepsilon_1)/(t_2 - t_1)$. When, for example, $t_2 - t_1 = 10^5 \text{ s}$ (1 day) and $\dot{\varepsilon} = 10^{-12} \text{ s}^{-1}$, $\varepsilon_2 - \varepsilon_1 = 10^{-7}$. Therefore, a reasonable assessment of weekly strain rate demands that strain must be measured with an accuracy of approximately 10^{-7} . Because the sample height of the specimen tested for this study is $h = 0.14 \text{ m}$, axial displacements must be measured with an accuracy of approximately 10^{-8} m .

3.5 Requirements when Performing Slow Creep Tests

It can be concluded from the discussion above that accurate long-term creep tests at low deviatoric stresses are possible only when the following requirements are met.

- The temperature and hygrometry changes are very small.
- The applied load can be controlled with high accuracy.
- The change in sample height can be measured with high resolution.

How these issues were addressed is described in the following Section.

4 A Creep Test in the Varangville Mine

4.1 Samples and Loading

A multistage uniaxial creep test was performed on a 70-mm-diameter and 140-mm-tall cylindrical salt sample. The sample was set between two duralumin platens (Fig. 6). Axial loads were applied to the specimen using dead weights placed on the lower part of a rigid frame below the sample. The use of dead weights ensures that load control is virtually perfect. The frame weight is transmitted to the upper duralumin plate through a small metallic ball. Because large stress concentration develops at the ball/platen interfaces, punching and wear of the platens by the ball were a concern. To lessen this concern, grease was applied between the ball and the platens before the test was initiated. The applied stress is equal to the overall weight of the steel frame divided by the initial cross-sectional area of the salt cylinder. Because strains are small throughout the test, no correction of the sample cross-sectional area was deemed necessary. Axial stress that can be applied to a sample using this apparatus ranges between 0.05 and 1 MPa.

4.2 Axial Displacement Gages

During the test, four high-resolution displacement sensors (Solartron linear encoders) were positioned in two orthogonal vertical planes (Fig. 6). The sensors provide four independent displacement measurements of the upper platen. Sensors accuracy is $0.5 \mu\text{m}$, and their resolution is $0.0125 \mu\text{m}$ ($1/80 \mu\text{m}$). The encoders operate on the

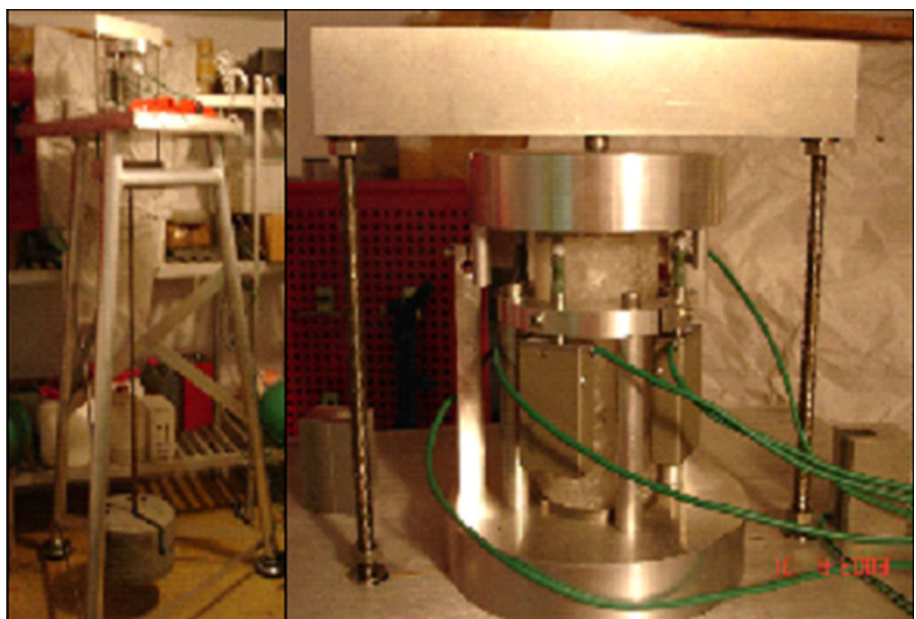
principle of interference between two diffraction gratings. Gratings are deposited on a quartz substrate. The gratings are composed of black and white rectangles of length $10 \mu\text{m}$. A first grating is illuminated by a light-emitting diode. A second grating is used to scan the modulated light intensity generated when the first grating moves as a consequence of sample deformation. The system computes displacements based on the number of rectangular intervals that crossed a stationary reference. A drawback of this system is that the counting is reset to zero whenever there is an electric outage. A couple of electric outages occurred inadvertently as a result of staff member activity in the room. Fortunately, corresponding offsets could be reconstructed to provide continuous strain-versus-time curves throughout the duration of the test (see Sect. 4.1).

Only three sensors are needed to allow both the relative rotation and vertical displacement of the upper plate to be measured. However, four sensors were used to provide some degree of redundancy.

4.3 Rotation of the Upper Platen

An example of upper plate rotation measured by the apparatus is provided in Fig. 7. Displacements u_1 , u_2 , u_3 , and u_4 of the four vertical sensors (A1, A2, A3, and A4) were measured during the initial 6 months of a test performed on an Avery Island salt sample in the Altaussee Mine. The four curves are different, which raises concerns about gage accuracy. However, it can be observed that the two curves $(u_2 + u_4)/2$ and $(u_1 + u_3)/2$, almost perfectly overlap, which proves that the four measured displacements are consistent, and strongly suggests that the upper

Fig. 6 Testing device and salt sample below the upper platen



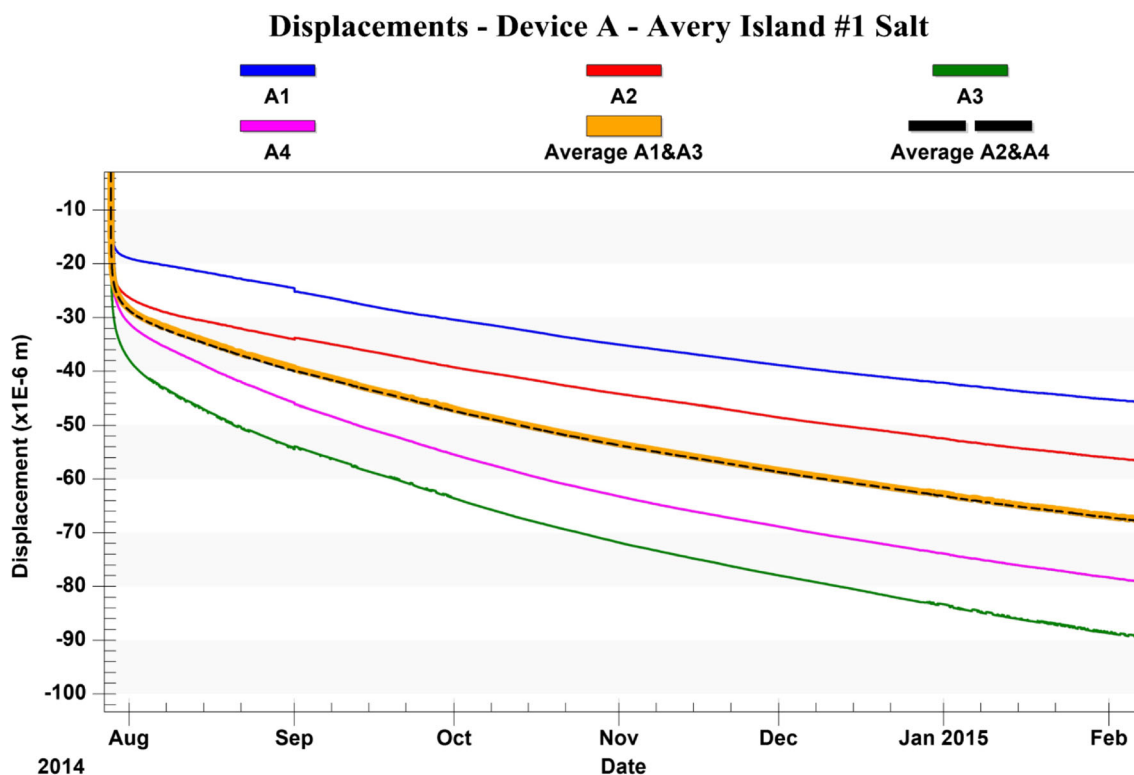


Fig. 7 Test on an Avery Island salt sample performed in the Altaussee Mine, depicting upper platen rotation

platen experiences a rigid displacement (a small rotation). This consistency also suggests that sensor drift is small.

4.4 Displacement Sensor Drift

To confirm that no sensor drift takes place, a duralumin cylindrical sample (instead of a salt sample) was placed in a similar testing apparatus from October 20, 2010, to November 30, 2010, and a 0.15 MPa load was applied. The strain rate of the duralumin sample at the end of November was less than $3 \times 10^{-13} \text{ s}^{-1}$, but it was faster at the beginning of the test. It is postulated that the strain rate was not zero because small irregularities on the duralumin-platen interface were being crushed under this load. Had the test been performed longer, all the asperities would have been destroyed and straining would have ceased. To verify this hypothesis, a longer test using a duralumin sample is planned.

4.5 Temperature Fluctuations

Temperature changes during a long-term creep test must be minimized because they are the main source of strain fluctuations. For this reason, the test was performed in a deep underground room where temperature is much more constant than in any surface facility. With the kind support of the Compagnie des Salins du Midi et Salines de l'Est, this and other tests have been performed at the dead end of

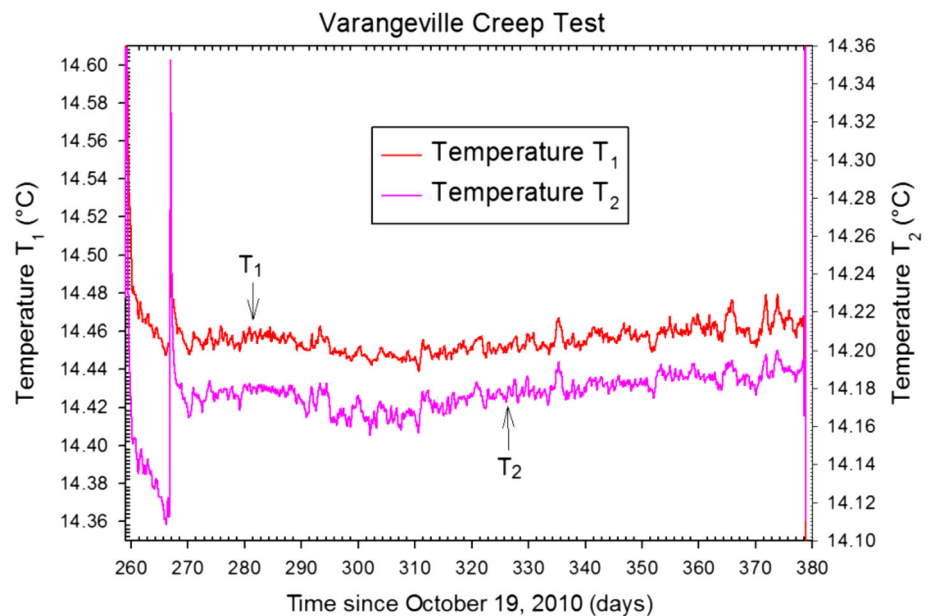
a 700-m-long, 160-m-deep drift of the Varangéville Mine in eastern France (Fig. 8). This gallery is remote from the area of present salt extraction. To supplement this test, a concurrent testing program, supported by the Solution Mining Research Institute, is being performed at the Altaussee salt mine in Austria.

Temperature is measured by platinum sensors with a resolution of one-thousandth of a degree Celsius; however, their accuracy is not better than 0.5 °C. As an example, temperature evolutions measured using two gages in the dead-end gallery at the Varangéville Mine between July 2011 and November 2011 are illustrated in Fig. 9. An offset clearly is visible, but more importantly, temperature fluctuations are parallel, which provides some confidence in gage resolution. Large temperature changes are visible when members of the staff were working in the gallery on day 266 (July 11, 2011). A slow temperature increase of 0.1 °C/year can be observed during the fall season beginning in early August. Relatively small erratic daily temperature changes also are observed. Such thermal stability was a surprise because changes in atmospheric pressure were expected to result in greater temperature fluctuations than those measured. Atmospheric pressure experiences fluctuations that can be as large as several hPa/day. In principle, a pressure increase will generate a temperature increase. When pressure changes are adiabatic, $dP_{\text{atm}}/P_{\text{atm}} = \gamma dT/(\gamma - 1)T$, where $\gamma = 1.4$, or $dT/$

Fig. 8 The testing devices at the gallery's dead end



Fig. 9 Temperature in the gallery from day 260 to day 380 (after October 19, 2010)



$dP_{\text{atm}} = 0.08^\circ\text{C/hPa}$, significantly more than the fluctuations measured at the mine. In fact, the adiabatic assumption is incorrect: mine temperature fluctuations are small because heat resulting from air compression is dissipated rapidly through the gallery walls; the thermal diffusivity of salt is not especially high ($k_{\text{salt}} = 3 \times 10^{-6} \text{m}^2/\text{s}$), but the thermal capacity of air is smaller than the thermal capacity of salt by three orders of magnitude, and the thermal inertia of air is quite large.

4.6 Correlation Between Strains and Temperature

As shown in Fig. 9, the drift temperature is quite stable, varying only of a few hundreds of a degree Celsius.

Because temperature is measured with a resolution of 0.001°C , one can attempt to correct the observed strain rate ($\dot{\epsilon}$) from the effects of temperature variations to obtain a better estimate for the viscoplastic strain rate. However, such a correction is possible only when long periods of time (several days) are considered. This is because a change in a drift's air temperature is not transferred immediately to the salt sample, as thermal conduction is a relatively slow process. For a sample diameter $D = 70 \text{mm}$, the characteristic time for heat conduction through the sample is $t_c = D^2/k_{\text{salt}} \approx 30 \text{minutes}$. When short-term fluctuations are considered, a time lag can be observed, and the apparent coefficient of thermal expansion is much smaller than expected. Better correlation is

observed if longer periods (weeks or months) are considered. An example of this is given in Fig. 10, which displays the as-observed temperature and strain during an earlier test at the Varangéville Mine. On day 133, a lamp inadvertently remained on and warmed the air in the drift, and an increase in temperature and a decrease in measured strain resulted. From day 150 to day 180, the temperature change is much more consistent (the temperature is decreasing slowly at a nearly constant rate before and after the incident), and a clear correlation can be established. The correction is $\alpha\dot{T} = 10^{-13}\text{s}^{-1}$. Correction is relatively poor when the light is on because, as mentioned above, temperature changes are fast during this period.

5 Test Results

5.1 A Multistage Creep Test

A multistage uniaxial creep test on an Avery Island salt sample was initiated on July 11, 2011 (A in Fig. 11). The initial axial load was 0.1 MPa and was increased to 0.2 MPa on March 14, 2012 (B in Fig. 11), to 0.3 MPa on November 7, 2012 (D in Fig. 11), and to 0.5 MPa on March 27, 2014 (H in Fig. 11). The first two stages and the fourth stage lasted approximately 8 months, while the third stage lasted approximately 15 months.

Temperature and hygrometry fluctuations, together with average strain evolutions determined from the four displacement sensors, are represented in Fig. 11. The hygrometer was out of order at the beginning of the test and was reinstalled on April 23–25, 2012 (C in Fig. 11). Later, humidity dropped from $\Phi = 75\%$ RH (a high figure that is suspect) to $\Phi = 68\%$ RH.

During this 42-month period, temperature fluctuations are smaller than $\pm 0.04\text{ }^\circ\text{C}$ (Fig. 11), except during short

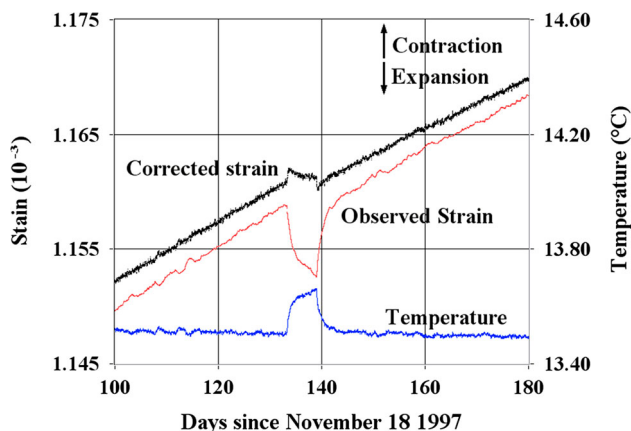


Fig. 10 Temperature and strain during an earlier test performed in 1997

periods when members of the staff worked in the gallery [April 23–25, 2012 (C in Fig. 11), November 7, 2013 (D in Fig. 11), June 5, 2012 (E in Fig. 11)], and January 28, 2014 [G in Fig. 11]. A long electric outage took place from G to H. Other than a small discontinuity of unknown origin in the strain-versus-time curve (F in Fig. 11), the strain data exhibit excellent quality.

5.2 Transient Strains

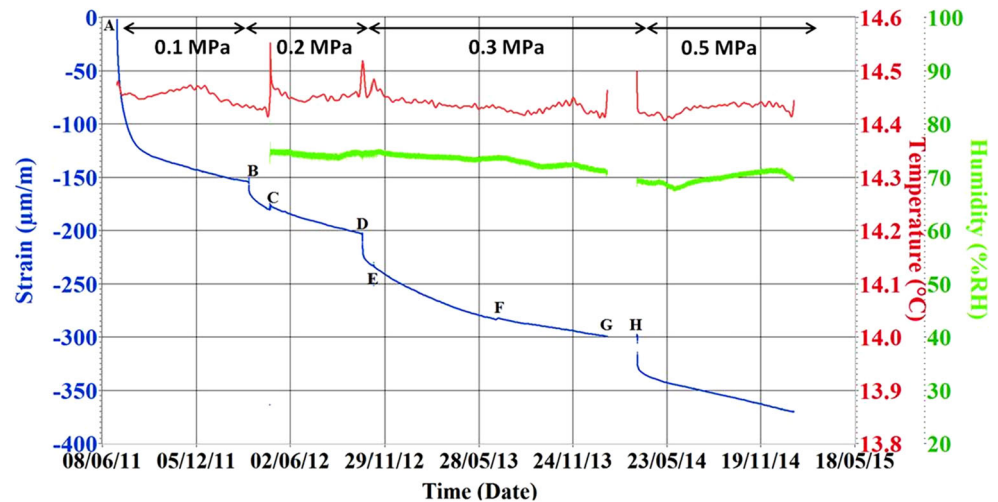
Reconciliation of displacement offsets during electrical outages that occurred on April 23–25, 2012 (point C), June 5, 2012 (point E), and January 24, 2014 (point G) was performed on the data presented in Fig. 11 to make the strain-versus-time curve smooth, as explained in Sect. 3.2. As illustrated in Fig. 11, large transient strains develop immediately after each load change (A, B, D, and H in Fig. 11). As exhibited by Eq 3, Munson et al. (1996) predict that the accumulated transient strain is a non-linear function of the applied stress, $\epsilon_t^* = K_0 e^{cT} \sigma^m$ (typically, $m = 3$). This model predicts that when applied stress is increased by a factor of 2, the accumulated transient strain, ϵ_t^* , should increase by a factor of 8. In other words, the accumulated transient strain should be much larger at the end of the second stage (when $\sigma_{zz} = 0.2$ MPa) than at the end of the first stage (when $\sigma_{zz} = 0.1$ MPa). In fact, this is not true. It is believed that, at the beginning of the test, the upper and lower faces of the sample were not perfectly flat, and small irregularities were crushed when the first load was applied. These irregularities were measured at a height or depth of $\pm 8\text{ }\mu\text{m}$.

5.3 Steady-State Strain Rates

Estimates for steady-state strain rate were computed for each of the four stress conditions specified for the test. Steady state was assumed to be reached within 8 months of applying each load. The average strain rate during the 20 days concluding 8 months of testing under the prescribed load was used in the rate estimation. The computed steady-state strain rates are $0.99 \times 10^{-12}\text{ s}^{-1}$ when $\sigma_{zz} = 0.1$ MPa, $1.59 \times 10^{-12}\text{ s}^{-1}$ when $\sigma_{zz} = 0.2$ MPa, $1.57 \times 10^{-12}\text{ s}^{-1}$ when $\sigma_{zz} = 0.3$ MPa, and $1.14 \times 10^{-12}\text{ s}^{-1}$ when $\sigma_{zz} = 0.5$ MPa. (The aforementioned rates are not corrected for temperature variations, whose effects are more than an order of magnitude smaller). These rates are of the same order of magnitude (10^{-12} s^{-1}) as the rates ($1.4 \times 10^{-12}\text{ s}^{-1}$ – $1.8 \times 10^{-12}\text{ s}^{-1}$) observed during similar tests performed 10 years earlier (Bérest et al. 2005) on an Etrez salt sample (rather than Avery Island sample) in the same gallery.

The strain rates during stages 3 and 4 are slower than that of stage 2 performed at a lower deviatoric stress. This

Fig. 11 Strain, humidity, and room temperature as a function of time during the test performed on an AI salt sample



response was unexpected and perplexing. A drop in hygrometry from $\Phi = 75$ %RH to $\Phi = 68$ %RH was observed during this period (accuracy of the hygrometer sensor is poor; however its resolution is fairly good). When Eq 6 is applied, a drop by $\Delta\Phi = -7$ % leads to a decrease in steady-state rate of approximately 50 %, which might explain why the observed strain rate during this period is slower than expected.

The most striking result is that steady-state strain rates are faster than the strain rates that can be extrapolated from tests performed at larger stresses by a factor of 100–1000 (Fig. 2).

6 Conclusions

The findings at this stage can be summarized as follows.

- 1 A multistage creep test was performed on an Avery Island salt sample. The testing device was set up in a 160-m-deep room of the Varangéville Mine, where temperature is quite stable. Four stages were managed: the applied axial load was 0.1 MPa, 0.2 MPa, 0.3 MPa, and 0.5 MPa, respectively. Each stage was at least 8 months in duration.
- 2 A several-month-long transient creep response is exhibited following each load change. The cumulated transient creep is largest during the first stage—in fact, small irregularities of the upper and lower faces of the samples were likely crushing during the first stage.
- 3 Hygrometry dropped by -7 %RH during the last two stages of the test, which may explain why strain rates are slower during these two stages than expected.

After an 8-month-long period, the steady-state strain rates are of the order of $1 \times 10^{-12} \text{s}^{-1}$ to $1.7 \times 10^{-12} \text{s}^{-1}$.

These strain rates are much greater than what can be extrapolated from the standard creep tests performed under higher deviatoric stress.

Acknowledgments The authors are indebted to Compagnie des Salins du Midi et Salines de l'Est whose kind help has been instrumental. The Solution Mining Research Institute kindly accepted reproduction of Fig. 7, which was obtained in the framework of a contract “Very slow creep rate as a basis for cavern stability analysis”. Special thanks to Kathy Sikora.

References

- Bérest P (2013) The mechanical behavior of salt and salt caverns. In: Proc. Eurock 2013, 17–30. Balkema, Rotterdam
- Bérest P, Blum PA, Charpentier JP, Gharbi H, Valès F (2005) Very slow creep tests on rock samples. *Int J Rock Mech Min Sci* 42:569–576
- Bérest P, Brouard B, Karimi-Jafari M, Van Sambeek L (2007) Transient behavior of salt caverns. Interpretation of Mechanical Integrity Tests. *Int J Rock Mech Min Sci* 44:767–786
- Blum W, Fleischman C (1988) On the deformation-mechanism map of rock salt. In: Proc 2nd Conf Mech Beh of Salt, 7–23. Trans Tech Pub, Clausthal-Zellerfeld
- Djizanne-Djakeun H (2014) Mechanical stability of a salt cavern submitted to rapid pressure changes. Dissertation, Ecole Polytechnique (in French)
- Horseman, S.T. (1988) Moisture content —a major uncertainty in storage cavity closure prediction. In: Proc 2nd Conf Mech Beh of Salt, 53–68. Trans Tech Pub, Clausthal-Zellerfeld
- Hunsche U (1988) Measurement of creep in rock salt at small strain rates. In: Proc 2nd Conf Mech Beh of Salt, 187–196. Trans Tech Pub, Clausthal-Zellerfeld
- Hunsche U, Schultze O (1996) Effect of Humidity and Confining pressure on creep of rock salt. In: Proc 3rd Conf Mech Beh of Salt, 237–248. Trans Tech Pub, Clausthal-Zellerfeld
- Hunsche U, Schultze O (2002) Humidity induced creep and its relation to the dilatancy boundary. In: Proc 5th Conf Mech Beh of Salt, 73–87. Balkema, Rotterdam
- Langer M (1984) The rheological behaviour of rock salt. In: Proc 1st Conf Mech Beh of Salt, 201–240. Trans Tech Pub, Clausthal-Zellerfeld

- Munson DE, Dawson PR (1984) Salt constitutive modeling using mechanism maps. In: Proc 1st Conf Mech Beh of Salt, 717–737. Trans Tech Pub, Clausthal-Zellerfeld
- Munson DE, De Vries KL, Fossum AF, Callahan GD (1996) Extension of the Munson-Dawson model for treating stress drops in salt. In: Proc 3rd Conf Mech Beh of Salt: 31–44. Trans Tech Pub, Clausthal-Zellerfeld
- Spiers CJ, Schutjens PMTM, Brzesowsky RH, Peach CJ, Liezenberg JL, Zwart HJ (1990) Experimental determination of the constitutive parameters governing creep of rocksalt by pressure solution. *Deform Mech Rheol Tect, Geol Soc Special Publi* 54:215–227
- Urai JL, Spiers CJ (2007) The effect of grain boundary water on deformation mechanisms and rheology of rocksalt during long-term deformation. In: Proc 6th Conf Mech Beh of Salt, 149–158. Taylor & Francis Group, London
- Van Sambeek LL (2012) Measurements of humidity-enhanced salt creep in salt mines: proving the Joffe effect. In: Proc 7th Conf Mech Beh Salt: 179–184. Taylor & Francis, London
- Van Sambeek L, Fossum A, Callahan G, Ratigan J (1993) Salt mechanics: empirical and theoretical developments. In: Proc 7th Symp on Salt, Vol I:127–134. Elsevier, Amsterdam
- Wawersik WR, Preece DS (1984) Creep Testing of Salt—procedures, problems and suggestions. In: Proc 1st Conf Mech Beh Salt 421–449. Trans Tech Pub, Clausthal-Zellerfeld